Neurobiology of Disease

Abnormal Long-Range Neural Synchrony in a Maternal Immune Activation Animal Model of Schizophrenia

Desiree D. Dickerson, Amy R. Wolff, and David K. Bilkey
Psychology Department, University of Otago, Dunedin 9054, New Zealand

The synchrony of neural firing is believed to underlie the integration of information between and within neural networks in the brain. Abnormal synchronization of neural activity between distal brain regions has been proposed to underlie the core symptomatology in schizophrenia. This study investigated whether abnormal synchronization occurs between the medial prefrontal cortex (mPFC) and the hippocampus (HPC), two brain regions implicated in schizophrenia pathophysiology, using the maternal immune activation (MIA) animal model in rats. This neurodevelopmental model of schizophrenia is induced through a single injection of the synthetic immune system activator polyriboinosinic–polyribocytidylic acid, a synthetic analog of double-stranded RNA, a molecular pattern associated with viral infection, in pregnant rat dams. It is based on epidemiological evidence of increased risk of schizophrenia in adulthood after prenatal exposure to infection. In the present study, EEG coherence and neuronal phase-locking to underlying EEG were measured in freely moving MIA and control offspring. The MIA intervention produced significant reductions in mPFC–HPC EEG coherence that correlated with decreased prepulse inhibition of startle, a measure of sensory gating and a hallmark schizotypal behavioral measure. Furthermore, changes in the synchronization of neuronal firing to the underlying EEG were evident in the theta and low-gamma frequencies. Firing within a putative population of theta-modulated, gamma-entrained mPFC neurons was also reduced in MIA animals. Thus, MIA in rats produces a fundamental disruption in long-range neuronal synchrony in the brains of the adult offspring that models the disruption of synchrony observed in schizophrenia.

Introduction

The temporal synchronization of neural firing has been proposed to bind and integrate diverse neural processes within the brain (Singer, 1999; Buzsáki and Draguhn, 2004). A considerable body of evidence suggests that changes in neural synchronization within and between brain regions may underlie a range of the deficits observed in schizophrenia (Uhlhaas et al., 2006; Spencer et al., 2009).

Although significant recent advances have been made in understanding how abnormal synchrony might be linked to schizophrenia (Uhlhaas and Singer, 2010), the fundamental causal mechanisms remain unclear. Disruption of long-range neuronal synchrony has been demonstrated recently in the context of a genetic model of schizophrenia (Sigurdsson et al., 2010), but the contribution of environmental risk factors has yet to be examined. Epidemiological studies suggest that environmental insults that occur at critical periods of brain development, such as maternal infection during the prenatal period, are associated with long-lasting changes in brain development and function, subsequent adult neuropathology (Rees and Inder, 2005), and specifically an increased risk of schizophrenia, in the offspring (Weinberger, 1987; Mednick et al., 1988; Brown and Derkits, 2010). Because prenatal exposure to a variety of infections is associated with this increased risk (Brown et al., 2001, 2004; Babulas et al., 2006), maternal immune activation (MIA) is considered to be a critical initiating factor (Patterson, 2002).

In the present study, we examined the synchronization of neural activity in the MIA model of schizophrenia. Activation of the maternal immune response involves injecting pregnant rat dams with a single systemic injection of the cytokine inducer polyriboinosinic–polyribocytidylic acid (Poly I:C) at approximately midgestation. Subsequent disruption to the neurodevelopment of the fetus results in a syndrome of structural, functional, and behavioral schizophrenia-like abnormalities in the offspring, typically with characteristic latent postpubertal onset (Zuckerman and Weiner, 2003; Zuckerman et al., 2003; Meyer et al., 2005; Ozawa et al., 2006; Wolff and Bilkey, 2008). Many of these symptoms have been shown to be responsive to acute and/or chronic antipsychotic drug treatment (Zuckerman et al., 2003; Piontkewitz et al., 2009).

Long-range neuronal synchrony was investigated in the adult MIA offspring and compared with matched control animals in an open-field task. Synchrony was measured between the hippocampus (HPC) and medial prefrontal cortex (mPFC), two regions known to have significant structural, functional, and neurochemical abnormalities in schizophrenia (Harrison, 2004; Tan et al., 2007), as well as disrupted functional connectivity (Meyer-Lindenberg et al., 2005). Furthermore, sensory gating was measured as an indication of the degree of schizophrenia-like behavioral disruption in these animals. Decreased coherence of

Received June 15, 2010; revised July 9, 2010; accepted July 24, 2010.

This research was supported by grants from the Health Research Council of New Zealand and the Marsden Fund. We acknowledge Sara Illingworth for her contribution.

There are no conflicts of interest, financial or otherwise, to declare for any of the authors.

Correspondence should be addressed to David K. Bilkey, Psychology Department, University of Otago, P.O. Box 56, Dunedin 9054, New Zealand. E-mail: dbilkey@psy.otago.ac.nz.

DOI:10.1523/JNEUROSCI.3046-10.2010

 0270-6474/10/3012424-08$15.00/0

neural activity between mPFC and HPC were observed in the EEG recordings of MIA animals, indicative of a reduction in long-range synchrony. This change in synchrony was associated with reductions in sensory gating behavior. At the cellular level, phase-locking of mPFC single-neuron firing was also disrupted in terms of both timing and phase of firing to simultaneously recorded EEG.

Materials and Methods

All procedures and experiments were performed in accordance with ethical guidelines of the University of Otago Ethics Committee.

Animals

Twelve female Sprague Dawley rats obtained from the University of Otago Animal Breeding Station were mated at 3 months of age. While under halothane anesthesia, six experimental-group dams were injected with a single dose of Poly I:C (4.0 mg/kg, i.v.) dissolved in saline, whereas control group dams received vehicle, on gestational day 15. Pups were culled to give a litter size of six males and weaned on postpartum day 21. The 12 animals used in this experiment (six MIA and six control) were obtained from independent litters and dams. Animals were prepulse inhibition (PPI) tested from ~3 months of age and were at least 5 months of age at the time of electrode implantation for subsequent electrophysiological recordings. No other procedures were conducted during the interim period. Experimental animals were housed three to a cage within their treatment group before surgical procedures and maintained on *ad libitum* food and water on a 12 h light/dark cycle.

Prepulse inhibition

Deficits in sensorimotor gating are a hallmark measure of validity in animal models of schizophrenia (Swerdlow and Geyer, 1998; Weiss and Feldon, 2001) as the ability of a weak prestimulus to reduce the startle response to a loud acoustic stimulus (known as prepulse inhibition) is reduced in individuals with schizophrenia. Acoustic startle responses of the 12 animals (six MIA and six control) were measured in a startle chamber (SR Lab; San Diego Instruments) using methods described previously (Wolff and Bilkey, 2008, 2010). Briefly, animals were placed inside a Plexiglas holding cylinder, on a platform mounted onto a piezoelectric accelerometer, all housed within a lit, sound-attenuated chamber. The acoustic stimuli was controlled by a computer using SR Lab software and provided through a speaker within the chamber. Each session involved startle-only (120 dBA, 40 ms), prepulse-only (72, 76, 80, and 84 dBA, 20 ms), prepulse plus startle (at all prepulse intensities), and no stimulus (68 dBA background only). Sessions began with 11 startle-only trials), followed by six blocks of the 10 different trial types (presented in pseudorandom, counterbalanced order). Ten startle-only stimuli completed the procedure. The interval between prepulse and startle stimuli was maintained at a constant 100 ms, and intertrial intervals ranged between 8 and 23 s. Sessions lasted ~35 min.

Surgery and electrode implantation

The 12 animals tested for PPI were subsequently surgically implanted with an adjustable microdrive assembly for neuron recording using techniques we have described previously (Bilkey and Muir, 1999; Zironi et al., 2001; Kyd and Bilkey, 2003, 2005; Muir and Bilkey, 2003; Liu et al., 2004; Russell et al., 2006). Briefly, while anesthetized with a ketamine–domitor mixture, a miniature, moveable microdrive (Bilkey and Muir, 1999) containing seven recording electrodes (Formvar-coated, nichrome wires with 25 μm diameter; California Fine Wire) was chronically implanted into the mPFC targeting the deep layers of the prelimbic and infralimbic cortices [+3.2 mm anteroposterior (AP) and +0.6 mm mediolateral (ML) to bregma; 3.2 mm dorsoventral (DV) from dura] through drilled stereotaxic-guided trephines. Furthermore, one non-moveable 127-μm-diameter, nickel-chromium coated wire was implanted in the CA1 region of the dorsal HPC (−3.8 mm AP and 2.5 mm ML to bregma; 2.5 mm DV from dura) to record EEG from near the hippocampal fissure. The assembly was fastened to the skull with jeweler's screws and acrylic dental cement. Animals remained on *ad libitum* food and water supply until 2 weeks after surgery, at which time their food was reduced to maintain the animal at ~85% of their free-feeding weight to optimize behavior during the recording procedure.

Electrophysiological recordings

Extracellular spikes were recorded using the dacqUSB multichannel recording system (Axona Ltd.). Signals were buffered via a field effect transistor source-follower mounted to the head stage with a "quiet" electrode as an indifferent. Neuron activity was bandpass filtered (between 360 Hz and 7 kHz), amplified 100 times, and digitized at a 48 kHz sampling rate by the dacqUSB system. Neuronal signals were digitized when the spike on any channel exceeded a threshold set above the background noise levels and were then stored for offline analysis. EEG signals were referenced to a skull screw located anterior to bregma and contralateral to the mPFC electrode trephine, low-pass filtered at 500 Hz, and sampled at 4800 Hz. The position of the animals' head was monitored by a ceiling-mounted video camera connected to a tracking system that monitored infrared light-emitting diodes mounted on the head stage. Head position was sampled at 50 Hz, and positional information was made available to the dacqUSB system.

Recording apparatus and procedure

The experimental chamber was a black, plastic, circular tub with a floor diameter of 74 cm and a wall height of 56 cm. The room was lit by a low-level light source located at one side of the room. This was not directly visible to the animal while in the apparatus. Animals were handled for 3 d before experimentation and habituated for two 20-min sessions within the environment for 2 d before their first recording. Two 10-min recordings were then obtained each day (morning and evening) while animals foraged for chocolate hail in the familiar open-field environment. The electrode was advanced through the mPFC cell layer by 40 μm after each recording session.

Data analysis

Prepulse inhibition. PPI is calculated as percentage PPI using the formula $100 - (PP/S) \times 100$, where PP is the average response on prepulse plus startle trials, and S is the average response on startle-only trials. Percentage PPI data was only analyzed for the midrange 80 dBA prepulse intensity because this has been shown to provide the greatest differentiation between MIA and control animals as a result of reduced floor and ceiling effects (Wolff and Bilkey, 2008, 2010). One raw startle value was found to be 3 SDs from the mean of the remaining trials and was therefore removed before percentage PPI was calculated and replaced with a value estimated from the linear trend generated through the neighboring PPI values for that animal (Wolff and Bilkey, 2008, 2010). Startle response to the first startle-only trial was assessed, as was the average startle response across the six PPI testing blocks.

Single-unit (neuron) recording. Single-neuron activity was manually identified on the basis of spike waveform characteristics using an offline cluster cutting program (TINT; Axona Ltd.). Raw EEG, spike times, and positional and behavioral data were read into Matlab (MathWorks) for additional analysis. Basic neuronal firing properties and behavioral measures were calculated using an in-house program, MapInfo (D. Bilkey, University of Otago, Dunedin, New Zealand).

Power spectral analysis. An averaged power spectral density (PSD) was derived for both hippocampal and mPFC EEG using Welch's modified method of spectral estimation in Matlab. The PSD was calculated using a discrete Fourier transform with a 9600 Hz sample, moving hamming window, giving a resolution of 0.5 Hz. To allow for effective comparison across sessions and animals, data were normalized so that the integral of the PSD over the range of 2–100 Hz was equal to one, thereby accounting for variance in signal amplitude across recordings and animals as a result of factors such as electrode impedance and location (Russell et al., 2006). To quantify the differences in peak amplitude within each frequency band against the underlying broadband activity, an exponential curve was fitted to the PSD using the least squares method (Russell et al., 2006). The difference between the fitted curve and the PSD was then retained, and the amplitude and frequency of the peaks in this difference curve were measured in the delta (2–4 Hz), theta (4–12 Hz), beta (12–30 Hz),

and gamma (low, 30–48 Hz; high, 52–100 Hz) frequency bands. This entire procedure was conducted using an automated Matlab routine, and the results within each frequency band were then compared between control and MIA animals.

Coherence analysis. The coherence spectrum represents a series of correlation coefficients (squared) indicating the degree of consistency of two signals as a function of frequency (Srinivasan et al., 1999). Coherence values range from 0, in which the time series are completely independent, to 1, in which signals at a specific frequency range are identical. Coherence was calculated using the standard Matlab function mscohere (MathWorks), which derived the magnitude squared coherence estimate using Welch's averaged modified periodogram method. A frequency resolution of 0.5 Hz was available. The magnitude of coherence between the regions was then extracted for each of the frequency bands as above and compared. The peak coherence values within each band were averaged across all recordings for each animal, providing a mean coherence value for each animal within each frequency band.

Spike phase relationship. EEG phase was determined by bandpass filtering the data within the frequencies of interest [using a two-pole Butterworth filter with the filtfilt function (Matlab; MathWorks) to avoid phase shifts caused by the filtering process] and then applying the standard Hilbert transform. Phase zero was the positive peak of the waveform. To determine the strength of phase-locking and preferred phase of firing of an mPFC neuron to underlying EEG activity, each spike was given a phase of firing value with reference to the simultaneously recorded EEG within each frequency band, and then a measure of angular dispersion (mean vector length − r) and mean phase angle were calculated across all spikes (supplemental Fig. 1, available at www.jneurosci.org as supplemental material). The value of r provides a measure of the concentration of firing about the unit circle and varies inversely with the degree of dispersion within the data. It may vary from 0 (firing is so widely distributed that a mean angle cannot be described) to 1 (when all firing is concentrated at the same phase angle). The distribution of neuronal firing to both hippocampal and mPFC EEG was assessed using the Rayleigh's test for circular uniformity (Zar, 1999) to determine whether the phase of firing distribution was evenly (and therefore without significant mean direction) or unevenly distributed (and therefore possessing a significant mean direction) within the frequency bands of interest. The Watson–Williams parametric test for two samples of circular data (Zar, 1999) was used to quantify differences in phase angle between the two populations of neurons.

Histological procedures. After study completion, animals were deeply anesthetized with halothane and underwent transcardial perfusion. After fixation, 60 μm coronal sections were mounted and stained with thionin, and subsequent examination of these sections was used to verify the placement of the electrodes.

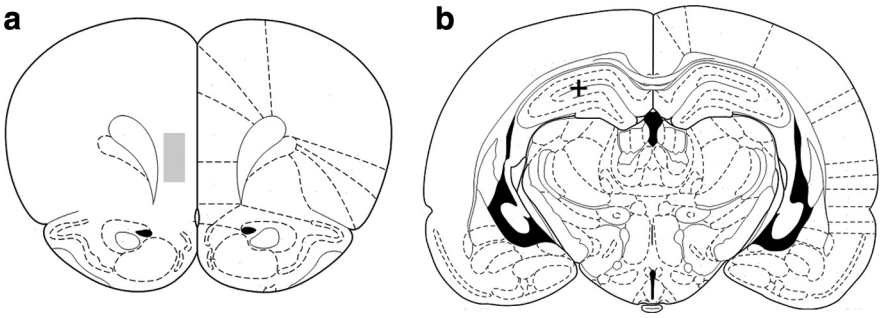

Figure 1. ***a***, mPFC electrodes targeted deep layers of prelimbic and infralimbic cortices (+3.2 mm AP and +0.6 mm ML to bregma; 3.2 mm DV from dura). The shaded box represents the region within which all the electrode tracts were located based on histology, starting coordinates, and distance that electrodes were moved. The cross in ***b*** shows the location of a typical lesion site marking the tip of the single EEG electrode in the dorsal hippocampus (CA1) (−3.8 mm AP and +2.5 mm ML to bregma; 2.5 mm DV from dura).

Results

Histological procedures confirmed electrode placement for both HPC and mPFC electrodes (Fig. 1). Average running speeds and area of the environment covered during recording were not found to differ between comparison groups. An ANOVA of speed data binned at 8 cm/s also revealed no significant group effect and no group × speed interaction (supplemental Fig. 2, available at www.jneurosci.org as supplemental material). Average electrode depths in the mPFC and spike amplitude were not found to differ between groups. Six MIA animals from six independent litters provided 47 EEG recordings, and 48 EEG recordings were obtained from six litter-matched control animals. Each recording was analyzed separately, and the results were averaged to obtain mean values for each animal within each frequency range.

MIA induces behavioral changes in offspring

The percentage PPI measure reflects the degree to which the low-amplitude prepulse stimulus inhibits startle behavior elicited by a later, high-amplitude stimulus. Analysis of startle behavior revealed a significant reduction in percentage PPI in the MIA animals ($t_{(9)} = -3.241$, $p = 0.01$) compared with control animals. Baseline startle reactivity in response to the startle stimulus alone was not different between treatment groups on the first startle-only trial ($p = 0.074$) or during the PPI testing blocks ($p = 0.3$).

MIA animals display reduced coherence between HPC and mPFC EEG that is correlated with behavioral deficits

Analysis of the mean peak coherence values revealed a significant reduction in coherence between the mPFC and HPC within the MIA group across most frequency bands investigated (Fig. 2*a*,*b*) (delta, $t_{(10)} = 3.05$, $p = 0.022$; theta, $t_{(10)} = 2.769$, $p = 0.02$; beta, $t_{(10)} = -3.188$, $p = 0.01$; and low-gamma, $t_{(10)} = 2.383$, $p = 0.038$). The frequency at which peak coherence occurred in the delta band was also significantly higher in MIA animals (supplemental Fig. 3, available at www.jneurosci.org as supplemental material) ($t_{(10)} = -2.33$, $p = 0.042$) but did not differ between groups in the theta, beta, and low-gamma bands. No significant difference in coherence or frequency was observed within the high-gamma band (52–100 Hz). Subsequent analysis of the theta frequency band revealed that the coherence differences were greater at the lower end of the frequency band (4–7 Hz) (Fig. 2*c*), in which coherence in MIA animals was significantly lower ($t_{(10)} = 2.404$, $p = 0.037$) than in controls. In contrast, no significant difference was observed in the high-theta (7–12 Hz) band, although there was a trend in the same direction. These reductions in long-range synchrony were not explained by major disruptions in either HPC or mPFC local activity, because analysis of the normalized PSD of the HPC and mPFC EEG revealed no differences between MIA and control recordings in regard to both the amplitude of the PSD peak or the frequency at which that peak occurred within any of the frequency bands investigated (Fig. 2*d*,*e*). Furthermore, the behavioral changes noted in the percentage PPI data (when pooled from the 11 animals; data from one control animal were not available) (Fig. 3*a*) reveal a positive linear relationship between the amount of EEG coherence measured

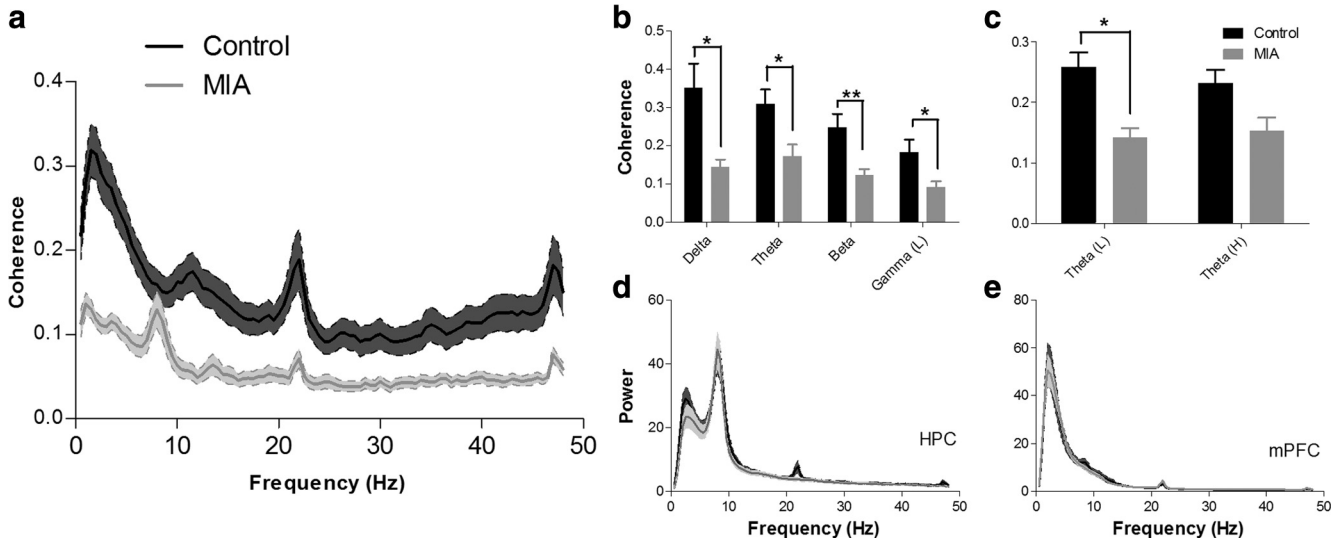

Figure 2. ***a***, Coherence spectrogram (mean ± SEM) of EEG simultaneously recorded from HPC and mPFC in control and MIA animals. There were significant reductions in coherence in the MIA animals in the delta, theta, beta, and low-gamma frequency bands as shown in ***b*** (mean ± SEM). A subsequent analysis (***c***) revealed that differences in coherence within the theta band primarily occur in the 4–7 Hz low-theta range. ***d***, ***e***, Mean ± SEM power spectral density plots of EEG from control and MIA animals recorded from the HPC and mPFC. MIA and control EEG recordings were found to have similar power across all frequency bands in both the HPC and mPFC recordings. $*p < 0.05$; $**p < 0.01$.

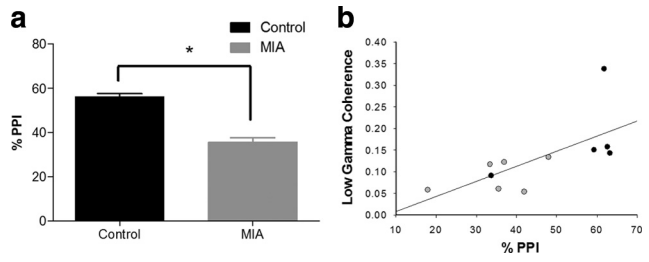

Figure 3. ***a***, Graph showing the sensory gating (%PPI) in control and MIA animals (mean ± SEM). There was a significant reduction ($*p < 0.05$) in the MIA group. ***b***, Scatter plot showing distribution of percentage PPI and low-gamma coherence (30–48 Hz) scores for MIA (gray) and control (black) animals (Spearman's rank order correlation coefficient, $r = 0.827$, $p < 0.001$). This effect was not driven solely by the highest coherence animal (top right data point) as with this data point removed ($r = 0.818$, $p = 0.002$).

in the low-gamma band and percentage PPI (Spearman's rank coefficient, $r = 0.827$, $p < 0.001$) (Fig. 3*b*).

mPFC neurons show decreased clustering and altered phase angle of firing to simultaneously recorded EEG

To investigate whether the reduction in synchrony between the HPC and mPFC observed in the MIA animal's coherence analysis was accompanied by changes at the single-neuron level, we examined the relationship between the firing of individual neurons in the mPFC and the simultaneously recorded EEG activity in both mPFC and HPC (Fig. 4*a*). A total of 98 neurons were recorded from the mPFC of MIA animals. These cells were isolated from 47 recording sessions in six animals derived from six independent litters. One hundred twelve cells were isolated over 48 recordings of six litter-matched control animals. The average number of neurons recorded from each animal was not found to differ between MIA and control animals, and the distribution of neurons between animals was similar across groups. The firing rate of mPFC neurons were found to differ significantly between groups, with neurons in MIA animals having a higher firing rate (1.79 ± 0.14 Hz) than control animals (1.26 ± 0.08 Hz; $t_{(207)} = 3.31$, $p < 0.01$). These firing rates are generally consistent with those reported in previous studies of mPFC neurons in free-foraging and place preference tasks (Jung et al., 1998; Hok et al., 2005). A Rayleigh's test revealed that MIA neurons showed decreased clustering of mPFC firing with reference to the HPC low-theta (5–7 Hz; $t_{(208)} = -2.161$, $p = 0.032$) and gamma (30–100 Hz; $t_{(208)} = -2.03$, $p = 0.022$) EEG cycles (Fig. 4*b*). The reduction in clustering of mPFC firing to the HPC gamma cycle was also significant when individual cell data were averaged and comparisons were made at the between-animal level ($t_{(10)} = 2.41$, $p = 0.037$). A significant reduction in clustering was also observed when mPFC neuron activity was referenced against theta oscillatory activity recorded in the mPFC in both the low-theta (5–7 Hz; $t_{(208)} = -3.015$, $p = 0.003$) and high-theta (7–9 Hz; $t_{(208)} = -2.132$, $p = 0.034$) frequency ranges (Fig. 4*c*).

In addition to changes in the clustering of firing, there was also evidence that the phase of neuronal firing was altered in the MIA animals. The results of a Watson–Williams test revealed significant between-group differences in the mean phase angle of firing of mPFC neurons to EEG signals recorded from both HPC and mPFC (Table 1). The mean phase angle to HPC EEG differed significantly within delta (2–4 Hz; $F_{(1,210)} = 28.58$, $p < 0.001$), theta (7–9 Hz; $F_{(1,210)} = 12.86$, $p < 0.001$), beta ($F_{(1,210)} = 37.5$, $p < 0.001$), and gamma ($F_{(1,210)} = 28.03$, $p < 0.001$) frequency bands. In control animals, mPFC neuron firing tended to occur on the negative-going phase of the HPC EEG cycle in theta, beta, and gamma frequency bands. In MIA animals, however, neurons tended to fire on the positive-going phase of the population oscillation in all four frequency bands. In relation to the mPFC EEG, the preferred phase of neuron firing again differed within the following frequency bands [mPFC; delta (2–4 Hz), $F_{(1,210)} = 27.69$, $p < 0.001$; theta (5–7 Hz), $F_{(1,210)} = 50.06$, $p < 0.001$; theta (7–9 Hz), $F_{(1,210)} = 5.10$, $p < 0.05$; beta, $F_{(1,210)} = 5.25$, $p < 0.05$], although the phase shift was less systematic.

Although the average firing rate of MIA neurons was significantly higher than control neurons, a Pearson's product moment correlation revealed no relationship between MIA neuron firing rate and coherence in any frequency band ($p > 0.05$). In control animals, however, average firing rate was shown to positively

correlate with coherence in the theta frequency band (Pearson's coefficient of 0.33, $p < .001$) but not in other bands. The absence of this positive relationship in neurons from MIA animals is notable ($F_{(1,419)} = 18.36$, $p < 0.0001$) compared with controls.

Reduced firing in theta-modulated, gamma-entrained mPFC neurons in MIA animals

The mean phase of firing of mPFC neurons to gamma frequency EEG recorded in the HPC was bimodally distributed in control animals, with one preferred firing phase occurring immediately after the peak of the gamma cycle and another just after the trough (Fig. 4*d*). In comparison, MIA neurons had a unimodal population distribution ($Z_{(1,197)} = 5.86$, $p = 0.0027$), preferring to fire near the gamma trough only (Fig. 4*e*). The firing phase histograms of individual control-group neurons were generally unimodal, indicating that the bimodal population distribution might be a result of two groups of neurons each tending to fire at different preferred phase angles. This suggested that one of these groups of neurons might not be active in MIA animals. To determine whether the control-group neurons could be defined on the basis of other characteristics, they were initially grouped depending on their phase of firing to gamma EEG (315° to 135° vs 135° to 315°). A comparison of firing properties of these two groups of neurons revealed no differences in average firing rate or in the running speed of the animal during activation. The spike amplitude (peak to trough) was, however, significantly higher in neurons that fired later in the gamma phase oscillation ($t_{(110)} = -2.502$, $p < 0.05$). One determinant of spike amplitude in extracellular recording is the distance from the electrode to the neuron. It is unlikely that this could account for these results, however, because there was no reason to expect the electrode tracks to preferentially pass close to certain neuron types and not others. Alternatively, however, changes in spike amplitude might reflect the influence of particular phasic inputs (e.g., shunting currents) on a certain subgroup of cells. These might differentially influence current flow that originates from action potentials but then propagates back into the dendrites (Stuart and Sakmann, 1994; Grewe et al., 2010) and so modulates the extracellular signal. The comparison also revealed a significant between-group difference in the relationship that these neurons had to the theta rhythm recorded in the mPFC. Those neurons that tended to fire near the peak of the mPFC gamma cycle showed significantly greater modulation of firing by mPFC theta activity (*r* value; 5–7 Hz, $t_{(110)} = -2.46$, $p = 0.015$; 7–9 Hz, $t_{(110)} = -4.0845$, $p < 0.001$) and a tendency to fire earlier in the theta cycle ($F_{(1,110)} = 46.29$, $p < 0.001$) compared with the population of neurons that fired at or just after the gamma trough. When MIA cells were categorized in the same way, this difference in theta modulation was not apparent. Furthermore, the relationship of spike amplitude to phase of firing to the gamma cycle in the mPFC was in the opposite direction in MIA neurons, such that neurons that tended to fire earlier had a higher spike amplitude ($t_{(95)} = -1.99$, $p < 0.05$) than those that fired later ($F_{(1,208)} = 9.93$, $p = 0.0019$).

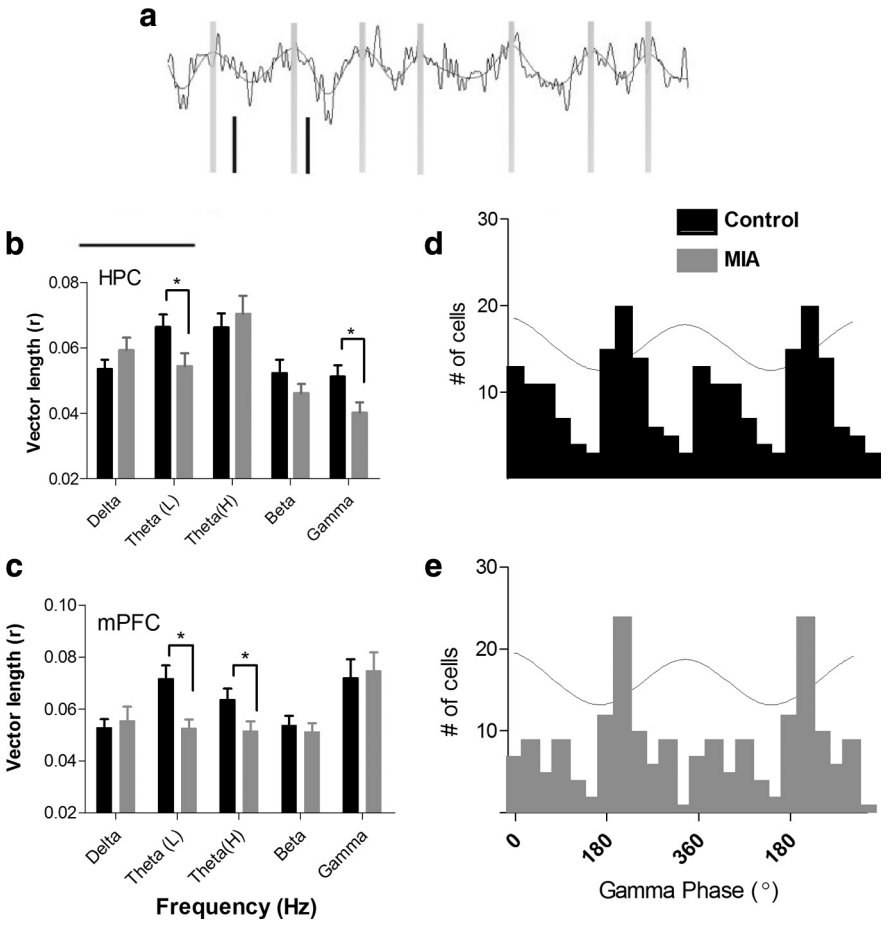

Figure 4. ***a***, Example of raw EEG recordings from HPC overlaid with the filtered theta oscillation. Zero phase is marked by gray vertical lines. The phase of firing of simultaneously recorded spikes from mPFC neurons are shown in black. ***b***, ***c***, When a firing phase analysis (supplemental Fig. 1, available at www.jneurosci.org as supplemental material) was applied to neurons recorded in the mPFC, a vector length (*r*) describing synchrony to the EEG was obtained for each cell. A higher *r* value indicates an increased concentration of firing about a particular phase of the EEG cycle. In several frequency bands, mPFC neurons from MIA animals show significantly reduced clustering of firing to the EEG recorded in the HPC (***b***) and mPFC (***c***). $*p < 0.05$; $**p < 0.01$. ***d***, ***e***, Histogram of preferred firing phase for all mPFC neurons referenced to HPC gamma EEG. Data are replicated over two cycles for visual clarity. The wave indicates the phase of the EEG cycle with 0° equal to the positive peak. A bimodal distribution across the 360° cycle is evident in the control population, which may indicate the presence of two populations of neurons with different firing phases. By comparison, the distribution of firing in MIA neurons is unimodal in nature. This may result from a reduction in firing in neurons with a preferred firing phase occurring just after the positive peak of the EEG.

Table 1. Mean phase angle of single-neuron firing to EEG

EEG source	Frequency band	Phase angle (°)		Phase difference	*F* value[a]
		Control	MIA		
HPC	Delta, 2–4 Hz	360	240	120	28.6***
	Theta, 5–7 Hz	199	257	58	3.1
	Theta, 7–9 Hz	180	260	80	12.9***
	Beta, 12–30 Hz	53	264	149	37.5***
	Gamma, 30–100 Hz	141	311	170	28.0***
mPFC	Delta, 2–4 Hz	37	295	102	27.7***
	Theta, 5–7 Hz	101	296	165	50.1***
	Theta, 7–9 Hz	360	249	111	5.1*
	Beta, 12–30 Hz	338	271	67	5.3*
	Gamma, 30–100 Hz	200	214	14	0.6

Mean phase angle of control and MIA mPFC neuron firing to HPC and mPFC EEG. $*p < 0.05$, $***p < 0.001$.

[a]The *F* value refers to Watson–Williams test comparisons between MIA and control animals.

Discussion

Prenatal environmental insult results in changes in long-range communication

The current study investigated neural synchronization between the HPC and mPFC in the MIA animal model of schizophrenia. The primary finding is that a single exposure to the viral mimic Poly I:C during pregnancy leads to a disruption in long-range synchronization of EEG activity between mPFC and HPC in the adult offspring of these animals. The change in synchrony occurred within the delta (2–4 Hz), theta (4–12 Hz), beta (12–30 Hz), and low-gamma (30–48 Hz) frequency bands. Furthermore, an analysis of single-neuron firing in mPFC also revealed that activity in MIA animals was disrupted in terms of both the timing and phase of firing to simultaneously recorded EEG. These effects were observed despite MIA animals showing no evidence of local disruptions to EEG activity in either the HPC or mPFC, nor were the observed effects explained by differences in basic neural properties, gross motor behavior, or differential learning patterns that might have resulted if task demands had been higher. The reductions in coherence and phase-locking evidenced here appear, therefore, to be a result of changes in long-range communication between the mPFC and HPC or an alteration in some third area that provides synchronization between these regions. These changes may also reflect an overall reduction in coherent oscillatory activity throughout a number of brain regions, in which the present findings may provide a window into a brain-wide abnormality in integration or communication between neural networks in schizophrenia.

MIA animals also displayed a significant reduction in sensorimotor gating, a behavioral deficit evident in individuals with schizophrenia and a hallmark indicator of schizotypal behavioral impairment in animal models of the disorder (Swerdlow and Geyer, 1998; Weiss and Feldon, 2001). Furthermore, there was a linear relationship between this behavior and coherence in the low-gamma frequency band. Oscillations in the gamma and beta frequency bands have been linked previously to the human sensory gating response (Müller et al., 2001; Johannesen et al., 2005; Hall et al., 2010). Furthermore, both the hippocampus (Zhang et al., 2002) and prefrontal cortex (Mears et al., 2006) have been implicated previously in the PPI response. It is unclear, however, whether the specific reduction in mPFC and HPC coherence is directly related to the impaired PPI responses or whether the change in coherence we observed reflects a more widespread deficit that might also influence processing in sensory and motor areas. Exploration of the coherence–PPI relationship in other brain areas would clarify this issue.

In addition to finding that abnormal long-range synchrony is produced in the MIA model, the current study provides evidence for a specific reduction in firing in a population of theta-modulated, gamma-entrained cells in the mPFC of MIA animals. It is possible that this putative group of cells may contribute to inter-region synchrony or be directly responsive to it. The subsequent reduction in cross-frequency coupling that resulted from this change may also play a role in some of the cognitive deficits observed in schizophrenia. For example, cross-frequency coupling has been related previously to performance in decision-making tasks (Tort et al., 2008), a process that is impaired in schizophrenia (Shurman et al., 2005; Heerey et al., 2008).

These findings are, to our knowledge, the first to provide evidence of disrupted long-range neural synchrony between distinct brain regions in an environmental risk model of schizophrenia. The results reported here parallel the disrupted neural synchrony described in the human schizophrenia literature and complement recent findings by Sigurdsson et al. (2010) showing that long-range synchrony is disrupted in the context of a genetic model of schizophrenia. Whereas this previous study reported a decrease in synchrony between the dorsal HPC and mPFC in the delta and theta frequency bands during a working memory task, here we report that disruptions also occur in the beta (12–30 Hz) and low-gamma (30–48 Hz) frequency ranges. The fact that the changes noted in the current study occur during a simple behavioral activity suggests that they represent a fundamental impairment. The gamma frequency disruption noted here is also of particular interest because changes in this band have been associated with schizophrenia in many studies. For example, reduced gamma synchrony has been associated with poorer perception (Kwon et al., 1999; Spencer et al., 2003, 2008; Spencer, 2008), working memory performance (Basar-Eroglu et al., 2007; Haenschel et al., 2009), and cognitive control (Cho et al., 2006).

At present, the degree to which local and distal synchronization are related phenomena is unclear (Uhlhaas and Singer, 2010). Previous studies have reported that disruption in local oscillatory activity can occur within some models of schizophrenia (Ehrlichman et al., 2009; Lodge et al., 2009; Belforte et al., 2010). This can, however, make the interpretation of between-region differences in coherence difficult because local disruptions in synchrony could influence long-range communication. The MIA animals in our study did not, however, have alterations in local PSD measures, rather the critical changes were in inter-region communication. The difference in local effects between this and previous studies may be attributable to the behavioral task. For example, Lodge et al. (2009), using the methylazoxymethanol acetate animal model, showed that disruption in local oscillatory activity occurred in both ventral HPC and mPFC during a conditioned fear response task. No difference was apparent, however, when recordings were made in a baseline open-field condition, a task similar to that used in the present study.

Putative molecular mechanisms

Several neurotransmitter systems play a crucial role in the generation and synchronization of cortical oscillatory activity, and abnormalities in these systems are implicated in the neuropathophysiology of schizophrenia (Lewis et al., 2005). In particular, GABAergic interneurons are known to phasically regulate pyramidal cell excitation through their dense perisomatic innervation of glutamatergic neurons. Through these connections, they can control network activity and produce synchronous oscillatory activity within various frequency bands (Cobb et al., 1995). One of the most consistent findings in postmortem studies of schizophrenia is a reduced expression of mRNA for the GABA-synthesizing enzyme glutamatic acid decarboxylase (or GAD_{67}) (Lewis et al., 2005). Furthermore, the disruption in oscillatory activity that is observed in schizophrenia has been linked to a subclass of GABAergic interneurons containing the calcium-binding protein parvalbumin (PV) (Lewis and Moghaddam, 2006; Sohal et al., 2009). Disruption to GABAergic signaling has also been demonstrated in the MIA model, with evidence for both a decreased expression of PV-containing interneurons and a suppression of the secretory glycoprotein Reelin, in both the HPC and mPFC regions of Poly I:C-treated mice (Meyer et al., 2008). Recent research within other animal models have reported a relationship between suppressed PV expression and disruption in local oscillatory activity (Cunningham et al., 2006; Lodge et al., 2009). It is possible, therefore, that the reductions in inhibitory signaling observed previously in the MIA model may be causally

related to the long-range disruption in coordinated neural activity described in the current study.

It is not yet clear, however, whether GABAergic disruptions are a precursor to, or a downstream product of, disruption to other neurochemical systems (Coyle, 2004; Uhlhaas and Singer, 2010). Impaired glutamatergic signaling via NMDA receptors has also been identified in the pathophysiology of schizophrenia (Goff and Coyle, 2001) and has been shown to play a role in the disruption of gamma frequency oscillation (Roopun et al., 2008; Ehrlichman et al., 2009; Belforte et al., 2010).

The disruption in synchronization evidenced here has been proposed to underlie a core dysfunction in the integration and binding of information in schizophrenia (Spencer et al., 2003; Uhlhaas and Singer, 2010). Abnormal synchronization has, for example, been related to a range of schizotypal behavioral deficits (Kwon et al., 1999; Lee et al., 2003; Cho et al., 2006; Uhlhaas et al., 2006; Pachou et al., 2008) (for review, see Uhlhaas and Singer, 2010). Although the above literature primarily identifies reductions in synchrony within the schizophrenia population, abnormal increases in synchronization have been correlated with increased presentation of positive symptomatology (Spencer et al., 2009). The present findings are in accord with the human schizophrenia literature and extend our understanding of possible mechanisms by highlighting the pervasive impact of an intrauterine environmental insult on long-range synchronization. These data, therefore, link an isolated environmental risk factor to the disrupted synchronization that may be a fundamental factor in the disease presentation.

References

Babulas V, Factor-Litvak P, Goetz R, Schaefer CA, Brown AS (2006) Prenatal exposure to maternal genital and reproductive infections and adult schizophrenia. Am J Psychiatry 163:927–929.

Basar-Eroglu C, Brand A, Hildebrandt H, Karolina Kedzior K, Mathes B, Schmiedt C (2007) Working memory related gamma oscillations in schizophrenia patients. Int J Psychophysiol 64:39–45.

Belforte JE, Zsiros V, Sklar ER, Jiang Z, Yu G, Li Y, Quinlan EM, Nakazawa K (2010) Postnatal NMDA receptor ablation in corticolimbic interneurons confers schizophrenia-like phenotypes. Nat Neurosci 13:76–83.

Bilkey DK, Muir GM (1999) A low cost, high precision subminiature microdrive for extracellular unit recording in behaving animals. J Neurosci Methods 92:87–90.

Brown AS, Derkits EJ (2010) Prenatal infection and schizophrenia: a review of epidemiologic and translational studies. Am J Psychiatry 167:261–280.

Brown AS, Cohen P, Harkavy-Friedman J, Babulas V, Malaspina D, Gorman JM, Susser ES (2001) A.E. Bennett Research Award. Prenatal rubella, premorbid abnormalities, and adult schizophrenia. Biol Psychiatry 49:473–486.

Brown AS, Begg MD, Gravenstein S, Schaefer CA, Wyatt RJ, Bresnahan M, Babulas VP, Susser ES (2004) Serologic evidence of prenatal influenza in the etiology of schizophrenia. Arch Gen Psychiatry 61:774–780.

Buzsáki G, Draguhn A (2004) Neuronal oscillations in cortical networks. Science 304:1926–1929.

Cho RY, Konecky RO, Carter CS (2006) Impairments in frontal cortical gamma synchrony and cognitive control in schizophrenia. Proc Natl Acad Sci U S A 103:19878–19883.

Cobb SR, Buhl EH, Halasy K, Paulsen O, Somogyi P (1995) Synchronization of neuronal activity in hippocampus by individual GABAergic interneurons. Nature 378:75–78.

Coyle JT (2004) The GABA-glutamate connection in schizophrenia: which is the proximate cause? Biochem Pharmacol 68:1507–1514.

Cunningham MO, Hunt J, Middleton S, LeBeau FE, Gillies MJ, Davies CH, Maycox PR, Whittington MA, Racca C (2006) Region-specific reduction in entorhinal gamma oscillations and parvalbumin-immunoreactive neurons in animal models of psychiatric illness. J Neurosci [Erratum (2006) 26:table of contents] 26:2767–2776.

Ehrlichman RS, Gandal MJ, Maxwell CR, Lazarewicz MT, Finkel LH, Contreras D, Turetsky BI, Siegel SJ (2009) *N*-methyl-D-aspartic acid receptor antagonist-induced frequency oscillations in mice recreate pattern of electrophysiological deficits in schizophrenia. Neuroscience 158:705–712.

Goff DC, Coyle JT (2001) The emerging role of glutamate in the pathophysiology and treatment of schizophrenia. Am J Psychiatry 158:1367–1377.

Grewe BF, Bonnan A, Frick A (2010) Back-propagation of physiological action potential output in dendrites of slender-tufted L5A pyramidal neurons. Front Cell Neurosci 4:13.

Haenschel C, Bittner RA, Waltz J, Haertling F, Wibral M, Singer W, Linden DE, Rodriguez E (2009) Cortical oscillatory activity is critical for working memory as revealed by deficits in early-onset schizophrenia. J Neurosci 29:9481–9489.

Hall MH, Taylor G, Salisbury DF, and Levy DL (2010) Sensory gating event-related potentials and oscillations in schizophrenia patients and their unaffected relatives. Schizophr Bull. Advance online publication. Retrieved August 18, 2010. doi:10.1093/schbul/sbq027.

Harrison PJ (2004) The hippocampus in schizophrenia: a review of the neuropathological evidence and its pathophysiological implications. Psychopharmacology (Berl) 174:151–162.

Heerey EA, Bell-Warren KR, Gold JM (2008) Decision-making impairments in the context of intact reward sensitivity in schizophrenia. Biol Psychiatry 64:62–69.

Hok V, Save E, Lenck-Santini PP, Poucet B (2005) Coding for spatial goals in the prelimbic/infralimbic area of the rat frontal cortex. Proc Natl Acad Sci U S A 102:4602–4607.

Johannesen JK, Kieffaber PD, O'Donnell BF, Shekhar A, Evans JD, Hetrick WP (2005) Contributions of subtype and spectral frequency analyses to the study of P50 ERP amplitude and suppression in schizophrenia. Schizophr Res 78:269–284.

Jung MW, Qin Y, McNaughton BL, Barnes CA (1998) Firing characteristics of deep layer neurons in prefrontal cortex in rats performing spatial working memory tasks. Cereb Cortex 8:437–450.

Kwon JS, O'Donnell BF, Wallenstein GV, Greene RW, Hirayasu Y, Nestor PG, Hasselmo ME, Potts GF, Shenton ME, McCarley RW (1999) Gamma frequency-range abnormalities to auditory stimulation in schizophrenia. Arch Gen Psychiatry 56:1001–1005.

Kyd RJ, Bilkey DK (2003) Prefrontal cortex lesions modify the spatial properties of hippocampal place cells. Cereb Cortex 13:444–451.

Kyd RJ, Bilkey DK (2005) Hippocampal place cells show increased sensitivity to changes in the local environment following prefrontal cortex lesions. Cereb Cortex 15:720–731.

Lee KH, Williams LM, Breakspear M, Gordon E (2003) Synchronous gamma activity: a review and contribution to an integrative neuroscience model of schizophrenia. Brain Res Brain Res Rev 41:57–78.

Lewis DA, Moghaddam B (2006) Cognitive dysfunction in schizophrenia: convergence of gamma-aminobutyric acid and glutamate alterations. Arch Neurol 63:1372–1376.

Lewis DA, Hashimoto T, Volk DW (2005) Cortical inhibitory neurons and schizophrenia. Nat Rev Neurosci 6:312–324.

Liu P, Jarrard LE, Bilkey DK (2004) Excitotoxic lesions of the pre- and parasubiculum disrupt the place fields of hippocampal pyramidal cells. Hippocampus 14:107–116.

Lodge DJ, Behrens MM, Grace AA (2009) A loss of parvalbumin-containing interneurons is associated with diminished oscillatory activity in an animal model of schizophrenia. J Neurosci 29:2344–2354.

Mears RP, Klein AC, Cromwell HC (2006) Auditory inhibitory gating in medial prefrontal cortex: single unit and local field potential analysis. Neuroscience 141:47–65.

Mednick SA, Machon RA, Huttunen MO, Bonett D (1988) Adult schizophrenia following prenatal exposure to an influenza epidemic. Arch Gen Psychiatry 45:189–192.

Meyer U, Feldon J, Schedlowski M, Yee BK (2005) Towards an immunoprecipitated neurodevelopmental animal model of schizophrenia. Neurosci Biobehav Rev 29:913–947.

Meyer U, Nyffeler M, Yee BK, Knuesel I, Feldon J (2008) Adult brain and behavioral pathological markers of prenatal immune challenge during early/middle and late fetal development in mice. Brain Behav Immun 22:469–486.

Meyer-Lindenberg AS, Olsen RK, Kohn PD, Brown T, Egan MF, Weinberger DR, Berman KF (2005) Regionally specific disturbance of dorsolateral prefrontal-hippocampal functional connectivity in schizophrenia. Arch Gen Psychiatry 62:379–386.

Muir GM, Bilkey DK (2003) Theta- and movement velocity-related firing of hippocampal neurons is disrupted by lesions centered on the perirhinal cortex. Hippocampus 13:93–108.
Müller MM, Keil A, Kissler J, Gruber T (2001) Suppression of the auditory middle-latency response and evoked gamma-band response in a paired-click paradigm. Exp Brain Res 136:474–479.
Ozawa K, Hashimoto K, Kishimoto T, Shimizu E, Ishikura H, Iyo M (2006) Immune activation during pregnancy in mice leads to dopaminergic hyperfunction and cognitive impairment in the offspring: a neurodevelopmental animal model of schizophrenia. Biol Psychiatry 59:546–554.
Pachou E, Vourkas M, Simos P, Smit D, Stam CJ, Tsirka V, Micheloyannis S (2008) Working memory in schizophrenia: an EEG study using power spectrum and coherence analysis to estimate cortical activation and network behavior. Brain Topogr 21:128–137.
Patterson PH (2002) Maternal infection: window on neuroimmune interactions in fetal brain development and mental illness. Curr Opin Neurobiol 12:115–118.
Piontkewitz Y, Assaf Y, Weiner I (2009) Clozapine administration in adolescence prevents postpubertal emergence of brain structural pathology in an animal model of schizophrenia. Biol Psychiatry 66:1038–1046.
Rees S, Inder T (2005) Fetal and neonatal origins of altered brain development. Early Hum Dev 81:753–761.
Roopun AK, Cunningham MO, Racca C, Alter K, Traub RD, Whittington MA (2008) Region-specific changes in gamma and beta2 rhythms in NMDA receptor dysfunction models of schizophrenia. Schizophr Bull 34:962–973.
Russell NA, Horii A, Smith PF, Darlington CL, Bilkey DK (2006) Lesions of the vestibular system disrupt hippocampal theta rhythm in the rat. J Neurophysiol 96:4–14.
Shurman B, Horan WP, Nuechterlein KH (2005) Schizophrenia patients demonstrate a distinctive pattern of decision-making impairment on the Iowa Gambling Task. Schizophr Res 72:215–224.
Sigurdsson T, Stark KL, Karayiorgou M, Gogos JA, Gordon JA (2010) Impaired hippocampal-prefrontal synchrony in a genetic mouse model of schizophrenia. Nature 464:763–767.
Singer W (1999) Neuronal synchrony: a versatile code for the definition of relations? Neuron 24:111–125.
Sohal VS, Zhang F, Yizhar O, Deisseroth K (2009) Parvalbumin neurons and gamma rhythms enhance cortical circuit performance. Nature 459:698–702.
Spencer KM (2008) Visual gamma oscillations in schizophrenia: implications for understanding neural circuitry abnormalities. Clin EEG Neurosci 39:65–68.
Spencer KM, Nestor PG, Niznikiewicz MA, Salisbury DF, Shenton ME, McCarley RW (2003) Abnormal neural synchrony in schizophrenia. J Neurosci 23:7407–7411.
Spencer KM, Salisbury DF, Shenton ME, McCarley RW (2008) Gamma-band auditory steady-state responses are impaired in first episode psychosis. Biol Psychiatry 64:369–375.
Spencer KM, Niznikiewicz MA, Nestor PG, Shenton ME, McCarley RW (2009) Left auditory cortex gamma synchronization and auditory hallucination symptoms in schizophrenia. BMC Neurosci 10:85.
Srinivasan R, Russell DP, Edelman GM, Tononi G (1999) Increased synchronization of neuromagnetic responses during conscious perception. J Neurosci 19:5435–5448.
Stuart GJ, Sakmann B (1994) Active propagation of somatic action potentials into neocortical pyramidal cell dendrites. Nature 367:69–72.
Swerdlow NR, Geyer MA (1998) Using an animal model of deficient sensorimotor gating to study the pathophysiology and new treatments of schizophrenia. Schizophr Bull 24:285–301.
Tan HY, Callicott JH, Weinberger DR (2007) Dysfunctional and compensatory prefrontal cortical systems, genes and the pathogenesis of schizophrenia. Cereb Cortex 17 [Suppl 1]:i171–i181.
Tort AB, Kramer MA, Thorn C, Gibson DJ, Kubota Y, Graybiel AM, Kopell NJ (2008) Dynamic cross-frequency couplings of local field potential oscillations in rat striatum and hippocampus during performance of a T-maze task. Proc Natl Acad Sci U S A 105:20517–20522.
Uhlhaas PJ, Singer W (2010) Abnormal neural oscillations and synchrony in schizophrenia. Nat Rev Neurosci 11:100–113.
Uhlhaas PJ, Linden DE, Singer W, Haenschel C, Lindner M, Maurer K, Rodriguez E (2006) Dysfunctional long-range coordination of neural activity during Gestalt perception in schizophrenia. J Neurosci 26:8168–8175.
Weinberger DR (1987) Implications of normal brain development for the pathogenesis of schizophrenia. Arch Gen Psychiatry 44:660–669.
Weiss IC, Feldon J (2001) Environmental animal models for sensorimotor gating deficiencies in schizophrenia: a review. Psychopharmacology (Berl) 156:305–326.
Wolff AR, Bilkey DK (2010) The maternal immune activation (MIA) model of schizophrenia produces pre-pulse inhibition (PPI) deficits in both juvenile and adult rats but these effects are not associated with maternal weight loss. Behav Brain Res 213:323–327.
Wolff AR, Bilkey DK (2008) Immune activation during mid-gestation disrupts sensorimotor gating in rat offspring. Behav Brain Res 190:156–159.
Zar JH (1999) Biostatistical analysis, Ed 4. Upper Saddle River, NJ: Prentice Hall.
Zhang WN, Bast T, Feldon J (2002) Prepulse inhibition in rats with temporary inhibition/inactivation of ventral or dorsal hippocampus. Pharmacol Biochem Behav 73:929–940.
Zironi I, Iacovelli P, Aicardi G, Liu P, Bilkey DK (2001) Prefrontal cortex lesions augment the location-related firing properties of area TE/perirhinal cortex neurons in a working memory task. Cereb Cortex 11:1093–1100.
Zuckerman L, Weiner I (2003) Post-pubertal emergence of disrupted latent inhibition following prenatal immune activation. Psychopharmacology (Berl) 169:308–313.
Zuckerman L, Rehavi M, Nachman R, Weiner I (2003) Immune activation during pregnancy in rats leads to a postpubertal emergence of disrupted latent inhibition, dopaminergic hyperfunction, and altered limbic morphology in the offspring: a novel neurodevelopmental model of schizophrenia. Neuropsychopharmacology 28:1778–1789.